ARID ZONE JOURNAL OF ENGINEERING, TECHNOLOGY & ENVIRONMENT
AZOJETE December 2022. Vol. 18(4):597-610
Published by the Faculty of Engineering, University of Maiduguri, Maiduguri, Nigeria.
Print ISSN: 1596-2644, Electronic ISSN: 2545-5818
www.azojete.com.ng

ORIGINAL RESEARCH ARTICLE

SIMULATION ANALYSIS OF BENCHMARK AXIAL VELOCITY AFTER SUDDEN EXPANSION USING COMPUTATIONAL FLUID DYNAMICS

T. O. Onah[1], O. M. Egwuagu[1], R. E. Ozioko[1], S. Chukwujindu[1], A. M. Nwankwo*[2], I. A. Nnaji[1], C. C. Aka[2]

[1]*Department of Mechanical and Production Engineering, Enugu State University of Science and Technology, Enugu, Enugu State, Nigeria*
[2]*Department of Mechanical Engineering, Caritas University, Amorji-Nike, Emene Enugu, Enugu State, Nigeria*
**Corresponding author's email address: zubbymike@gmail.com*

ARTICLE INFORMATION

Submitted 14 June, 2022
Revised 22 July, 2022
Accepted 25 July, 2022

Keywords:
Computational Fluid Dynamics (CFD)
After sudden expansion
Axial Velocity
Models
Simulation

ABSTRACT

Computational Fluid Dynamics (CFD)- ANASYS 2020R1 was used for the analysis of food and drug administration (FDA) benchmark study for biomedical flow transition. An idealized medical device is presented within this study and the CFD predictions of pressure and velocity are compared against experimental measurements of pressure and velocity. The fluid flow transition considered for Reynold numbers(s) 500, 2000, and 6500 with turbulent fluid flow models- laminar, k-omega, k-omega SST and k-epsilon based on throat Reynolds number Re_{th}. 500, 2000 and 6500. Mesh independence K-omega SST model used at 0.0008, 0.0004 and 0.0002 element sizes showed good matched velocity of 5.9m/sec. This converged at 0.0002, which is 2% of total pressure drop. Axial velocity at centreline for Re_{th} 500, 2000 and 6500 at line X =0, showed maximum difference of 77.4% velocity centerline at 0.08m and 19% wall pressure at -0.09m sudden expansion laminar region of Re = 500. Besides, 65.6% and 17.2% obtained at transition Re =2000, showed good agreement between CFD simulations and experimental measurements, at turbulent region Re = 6500, all models were in good agreement at 49.6% velocity centerline and 8.10% pressure drop in laminar region. Also, downstream of the simulation of Re_{th} =6500, other models disappeared which demonstrated K-epsilon model is best at higher Reynolds region. The result revealed negligible pressure gradient at the center line of the wall pressure, and dropped at the normalization point of the experimental pressure data range of 0 to -120n/m^2 and balanced at the throat Reynolds number of Re_{th} = 500.

1.0 Introduction

In biomedical applications, computational fluid dynamics (CFD) is used in designing and analyzing medical device, which helps with the visualization of fluid flows for detection of particular problem, and providing insight into patterns within flow field. As such U.S. Food and Drug Administration (FDA) have designed a computational inter laboratory study (with 28 independent groups) to validate CFD techniques and produce experimental parameters to support CFD verification and validation (Huang, 2018). ANSYS was used to simulate prediction models for blood fluid flow transition for FDA which is one out of numerous techniques of solving numerical problems of Navier Stokes equations (NSE), which has found its needs in the fluid dynamics area of biomedical engineering (Bernsdorf et al., 2008, Jain et al., 2017, Sun and Mun, 2008, and Jain, 2020)

This technique represents and handles complex anatomical geometries with ease and also enables simulations on massively parallel computing architectures (Jain et al., 2017). Works of Jain (2020), Zhang et al. (2008), Jain et al. (2017) have been applied in Lattice Boltzmann's Method (LBM) for complex transitional flows of anatomical geometries and was found to be efficient and effective. However, effort has not been made to appraise its effectiveness in FDA nozzle benchmark area. It is overbearing, to discover suitability of benchmark using methods without application (White and Chong, 2011). LBM application to FDA nozzle benchmark was only for laminar cases. Previous works done on computation transition flow using LBM by Jain (2020), Jain et al. (2017) was for moderate Reynolds number. Therefore, there is need to evaluate simple LBM scheme, without employing complex collision synthetic models at turbulence inflow, to accurately predict benchmarked FDA result, Focus should be on the Reynold number categories of transition and turbulent flow regimes of ranges 2000 and 6500. Comparative analysis was for V*elocities,* shear stresses, pressures and jet breakdown location with simulations. U.S. Food and Drug Administration created an initiative to establish CFD simulation as a regulatory tool for medical scheme. Stewart et al. (2012) worked on two 'benchmark 'flow models with specific parameters which they tested for accurate provision of experimental datasets. Experimental results are a useful basis for validating accuracy of CFD simulation and assessing its capacity in development and improvement of medical device. This disquisition focuses on nozzle benchmark model and compares experimental measurement of pressure and velocity provided by Particle image velocimetry (PIV) testing and compares it against CFD results. The ideal medical device made up of four sections: inlet tube, gradual-change section, tube throat and outlet tube. Inlet tube and outlet tube have diameter of 0.012m, throat has a diameter of 0.004m. The cone-shaped "gradual-change" section connects the inlet with throat and has a length of 0.22685m, nozzle has a length of 0.04m. The flow will enter through inlet and then experience a gradual convergence and go through the narrow nozzle throat before it increases at expansion region and flows through the outlet tube. The outlet length is 30 times size of the diameter, 0.36m, which gives enough space for fluid flow full development. The inlet length is calculated using Equation 1 (Stewart et al., 2012):

$$L_e = 4.4D\ Re^{\frac{1}{6}} \quad (1)$$

where: L_e is inlet length in (mm), D is diameter in (mm) and Re is Reynolds Number

The numerical methodology employed were based on laminar, (Stewart et al., 2012), where flow rate and tube throat Reynolds number is 500, near transition and turbulent tube throat Reynolds number is 2000 and 6500, used for determination of free stream velocities that allowed calculating first layer height Y^+ (Stewart et al., 2012)

CFD is a valuable tool for characterizing velocity, pressure, and shear stress in flow fields by numerical techniques. Over 50 years, CFD application have extended in the areas of airfoil and automobile for observing any kind of flow around them to improvement and assessment of blood contacting medical devices (Burgreen et al., 2001 and Marsden et al., 2014). The advantages of CFD in designing medical device includes; it provides insight in performance without costly prototypes, providing data assessment at critical regions and predicting difficult measuring quantities which influence blood damage (Raben et al., 2016, Fraser et al., 2012). Although U.S. Food and Drug Administration have nothad CFD simulation on blood contacting medical device, heart valves international standard does (ISO 5840-2, 2015 and ISO 5840-3, 2013). ISO 14708-5 (2010) recognizes Implantable circulatory support device experimental validation with CFD simulation for flow fields characterization in and around these devices, and assess potentials of hemolytic and thrombogenic. However, NSAI (2012) for ISO 14708-

Corresponding author's e-mail address: zubbymike@gmail.com

5 and ISO 5840-2 (2015) standards indicate that CFD usage be limited to design stage which is more appropriate for evaluating relative changes than assessing absolute quantities in design (ISO 14708 - 5, 2010). CFD does not predict value of blood damage but predicts solutions to complex fluid flows, hence the focus on transitional flow regime of Reynolds number 2000 and 6500. Physical quantities of velocities, shear stresses, pressures and jet breakdown location are compared with simulations.

Evaluating other benchmark devices using computational studies requires FDA-specified test conditions. Particle image velocimetry (PIV), and hemolysis testing results from the first study on the nozzle model which previously has been disseminated through a series of publications (Stewart et al., 2012, Stewart et al., 2013 and Hariharan et al., 2011). This study aims at evaluating the FDA benchmarks for velocity analysis after sudden expansion using the blood pump model performance of 2D- axisymmetric model based on simulation models

2. Materials and Methods

The idealized medical device is made up of four sections: the inlet tube, the gradual-change section, the nozzle throat and the outlet tube. The inlet and outlet tube have a diameter of 0.012m, the throat has a diameter of 0.004m. The cone-shaped "gradual-change" section connects the inlet with the throat and has a length of 0.22685m, the nozzle throat has a length of 0.04m. the methods are, the flow enters the system through the inlet and experience a gradual convergence as it goes through the throat before it increases at the sudden expansion side and flows through the outlet tube. The length of the outlet is 30 times the size of the tube diameter, and this gives enough space for the full development of the flow. The benchmark nozzle model geometry was used as standard, ANSYS fluent simulation software. The three flow regimes Reynolds number values were, for the laminar (Re=500), transition (Re = 2000), and turbulent (Re = 6500). The fluid flow model in turbulence used were: the k-w model, k-w SST model, Spalat Allmaras model, Transition SST model, Laminar Model, K-e model and Reynolds stress model. The y plus values were for k-e and Reynolds Stress models and the rest of the models has y plus values as was given by the equation 1 above.

Equations 2 to 5 were used for Calculations. The velocities were calculated using the Reynolds Equation and the wall distance was calculated using Equations 3 to 5.

$$L_e = 4.4D\ Re^{\frac{1}{6}} \tag{2}$$

$$R_e = \frac{\rho U_{freestream} L_{boundary\ layer}}{\mu} \tag{3}$$

$$C_f = (2log_{10}(Re_x) - 0.65)^{-2.3}\ for\ Re_x < 10^9 \tag{4}$$

$$\tau_w = C_f . \frac{1}{2} \rho U_{freestream}{}^2$$

$$U_* = \sqrt{\frac{\tau_w}{\rho}} (4) y = \frac{y^+ \mu}{\rho u_*} \tag{5}$$

where: Re is Reynolds Number, C_f is the coefficient of friction U_* is the freestream velocity and τ_w is the wall shear stress. L_e is the inlet length in (mm), D is the diameter of tube (mm), Re is the Reynolds Numbers, C_f is the coefficient of friction, $\tau_w, and\ U\ is\ the\ freestream$, is the wall shear stress, and U is the freestream, ρ is the density of the fluid (kg/m^3), l is the boundary layer conditions.

Corresponding author's e-mail address: zubbymike@gmail.com

3. Results

3.1 Velocities and Wall distances

Table 1 shows the boundary conditions used for the models, which have the flow rate, inlet and throat Reynolds Numbers, and inlet and free stream velocities.

Table 1: Flow Boundary Conditions in the nozzle model

Flow rate (m^3/s)	Inlet *Re*	Throat *Re*	Inlet velocity u_0	Freestream velocity
5.21×10^6	167	500	0.0461 ms^{-1}	0.4143 m/s
2.08×10^5	667	2000	0.1842 ms^{-1}	1.6572 m/s
6.77×10^5	2167	6500	0.5985 ms^{-1}	5.3859 m/s

Table 2 shows the calculated wall distances according to flow conditions of the various Reynolds Numbers, when Y+ is 1 and 30

Table 2: Wall distance according to flow conditions

	Re =500	Re=2000	Re=6500
Wall distance (m) (when y+ =1)	6.8×10^{-5} m	2.2×10^{-5} m	8.1×10^{-6} m
Wall distance (m) (when+=30)	2.0×10^{-3} m	6.6×10^{-4} m	2.4×10^{-4}m

The Description of Nozzle Benchmark Model Design of A 2D-axisymmetric axial nozzle model geometry inlet length of 0.23m and out length of 0.36m, throat 0.04m (Figure 1), were created in solid work and imported in the Ansys work bench 2020R1, with incompressible fluid blood.

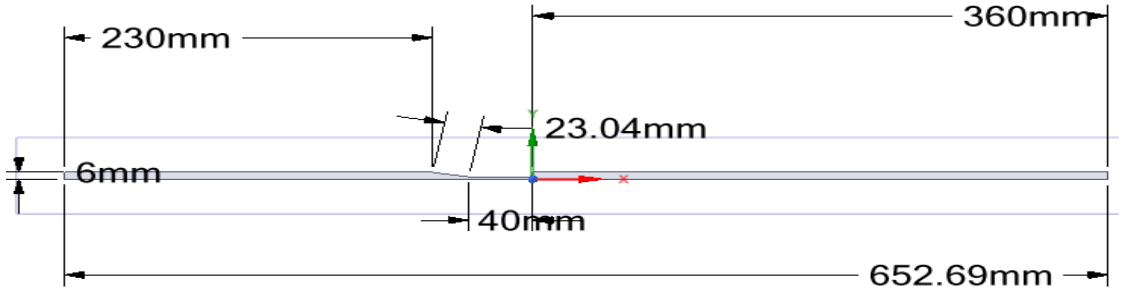

Figure 1: Geometry of 2D axisymmetric axial nozzle model

Then CFD FLUENT SOLVER edge sizing of Table 3 default growth rate used by pre-processor to generate meshes and Figures 2, 3 and 4 for each of 0.0008m, 0.0004m and 0.0002m element sizes, respectively.

Corresponding author's e-mail address: zubbymike@gmail.com

Table 3: Edge Sizing details

Details of "Edge Sizing" - Sizing	
Scope	
Scoping Method	Geometry Selection
Geometry	5 Edges
Definition	
Suppressed	No
Type	Element Size
Element Size	Default (3.2636e-002 m)
Advanced	
Behavior	Soft
Growth Rate	Default (1.2)
Capture Curvature	No
Capture Proximity	No
Bias Type	No Bias

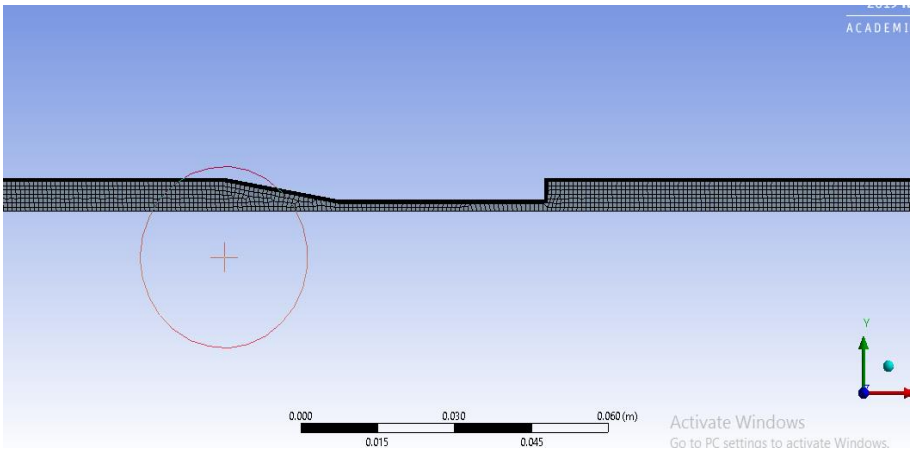

Figure 2: Mesh of element size 0.0008

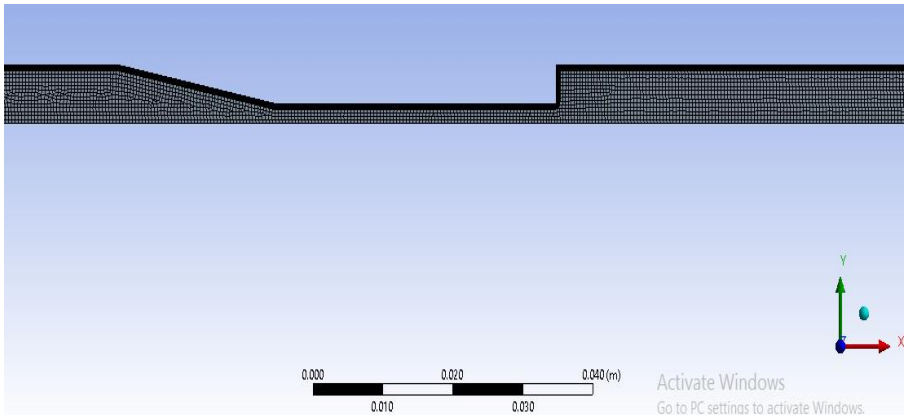

Figure 3: Mesh of element size 0.0004

Corresponding author's e-mail address: zubbymike@gmail.com

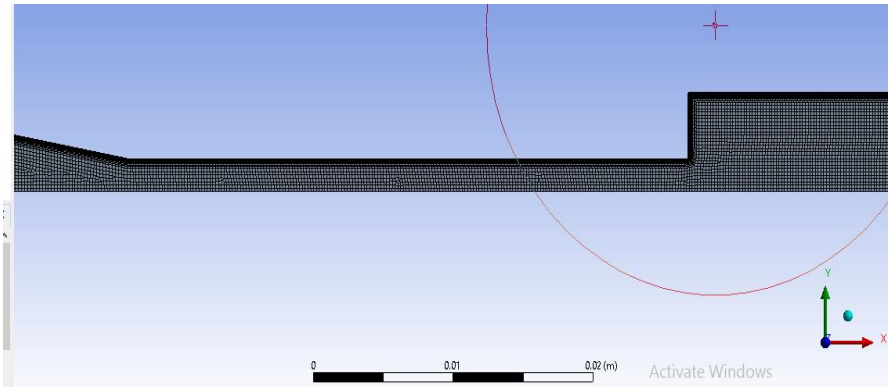

Figure 4: Mesh of element size 0.0002

The next which is set-up was used for the initialization and running calculation for 10000 iterations (Figures 5, 6 and 7). The accuracy of the numerical solution presented within this study is contingent on the accurateness of the mesh structure and Boundary conditions as specified in Table 1. Mesh convergence is an important part of ensuring that a solution is valid. By monitoring the residual RMS error and ensuring that variables (such as the pressure drop) do not significantly change with the refinement of the mesh. Table 4 shows information about the mesh sizes used when trying to solving the flow problem.

Table 4: Mesh Information

Element Size (m)	Nodes	Elements	Pressure Drop (Pa)
0.0008	13421	12647	21907
0.0004	34610	33169	21512
0.0002	112291	109651	21111

The K-ω SST model was chosen for the mesh independence study and the Reynolds number was chosen to be 6500 with an inlet velocity of 0.5985 ms^{-1}. The convergence criteria were set to $1x10^{-3}$ and a convergence tolerance of 10^{-7} was reached during the hybrid initialization. The residuals were given 1000 iterations to converge and although most of the plots converge around the 10^{-7} and show very good agreement the continuity plot plateaus at around $1.1 x10^{-3}$ for all the meshes. Figures 5, 6 and 7, thus illustrate the scaled residuals plot at different element sizes. 0.0008 takes 200 iterations to reach a steady-state whereas the other meshes reach a steady-state somewhere around the 150th iteration which is an indication of a higher degree of accuracy.

Corresponding author's e-mail address: zubbymike@gmail.com

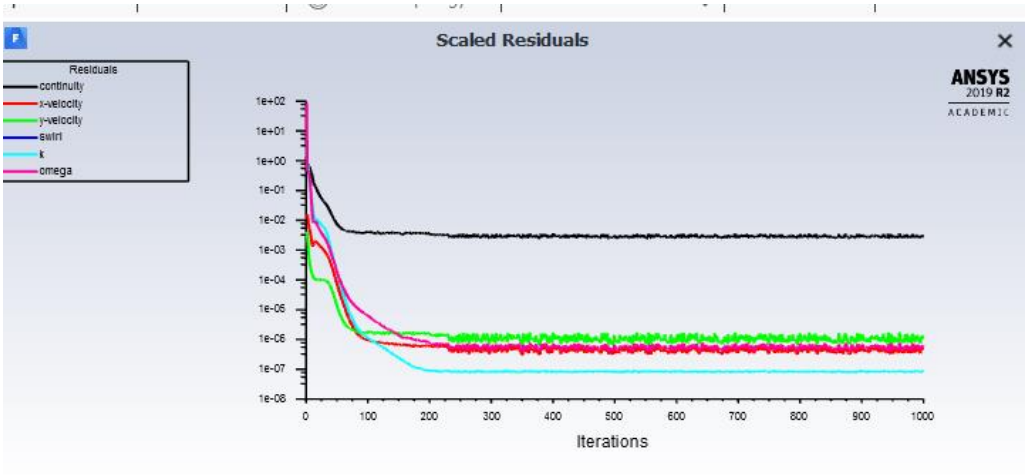

Figure 5: Simulation iteration of Scaled residual value for 0.0004 mesh

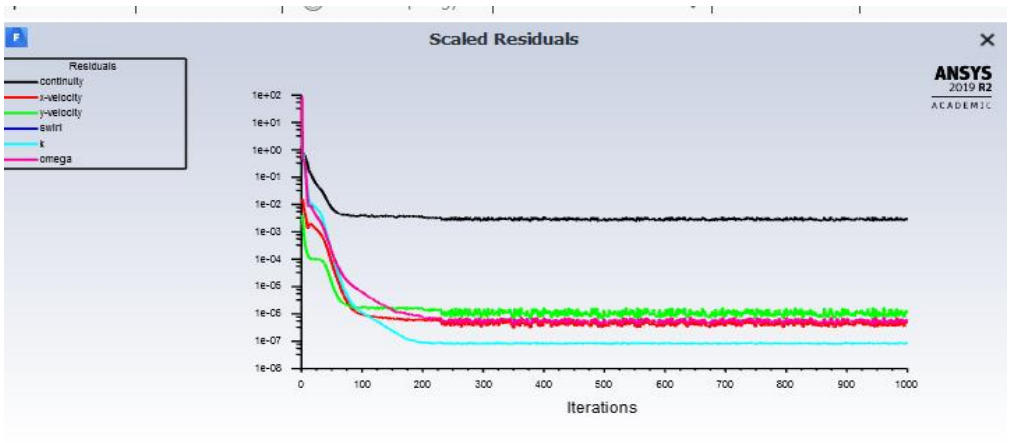

Figure 6: Simulation iteration of Scaled residual value for 0.0004 mesh

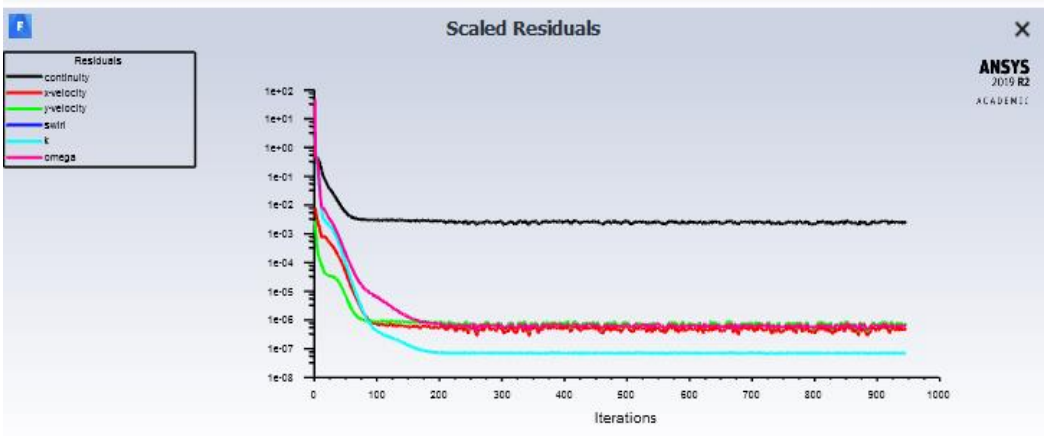

Figure 7: Simulation iteration of Scaled residual value for 0.0002 mesh

Figures 2, 3 and 4 show that the lower the element size, the higher the number of nodes and element number with decrease in pressure. Figures 5, 6, and 7 show the scaled residual values of the three element sizes, with average 200 number of iterations handles by the ANSYS before convergence.

The pressure and velocity contours of each element sizes are shown in Figures 8 9, 10, 11, 12, and 13, respectively. It shows that the velocity component of element size 0.0008 slowed down at 5.6m/s which is different from the velocities at same point of 0.0004 and 0.0002

Corresponding author's e-mail address: zubbymike@gmail.com

element sizes. However, velocities at 0.0004 and 0.0002 element sizes started at 6.6m/s and 6.59m/s with 0.01% difference and agreed at velocity 5.9m/s. Based on the inference, 0.0004 element size was now chosen as a mesh independence for subsequent analysis and simulation for determination of axial velocity at centreline, wall Pressure and axial velocity at different points using K-epsilon, Laminar, K-omega and K -omega-SST models. These effects of these models were studied at before and after the sudden expansion exchange of 0.02m as studied by Onah et al. (2022).

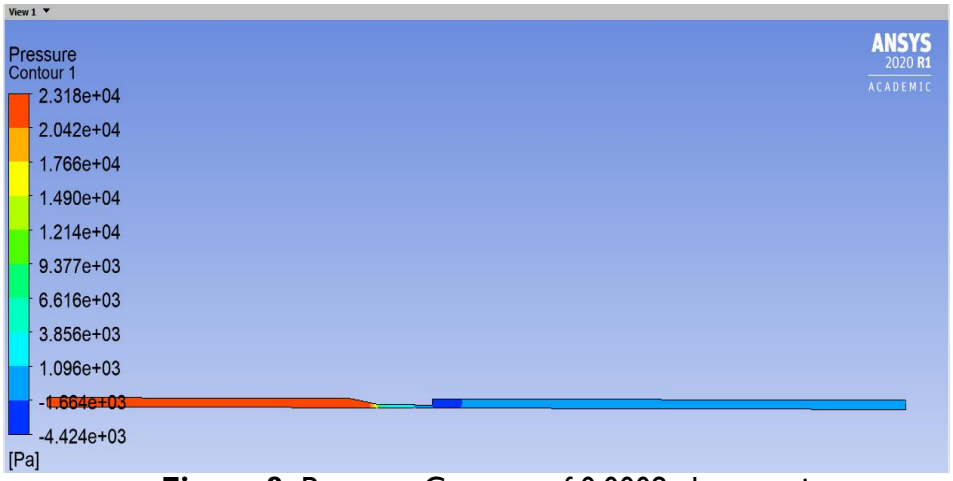

Figure 8: Pressure Contour of 0.0008 element size

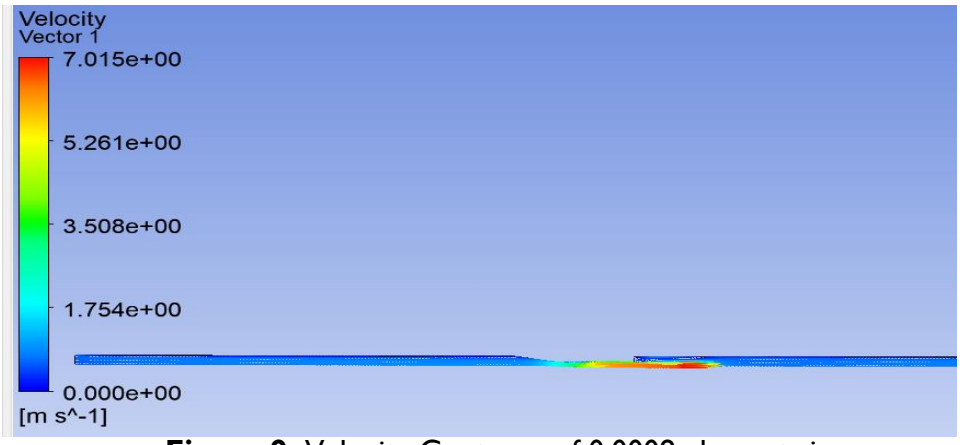

Figure 9: Velocity Contours of 0.0008 element size

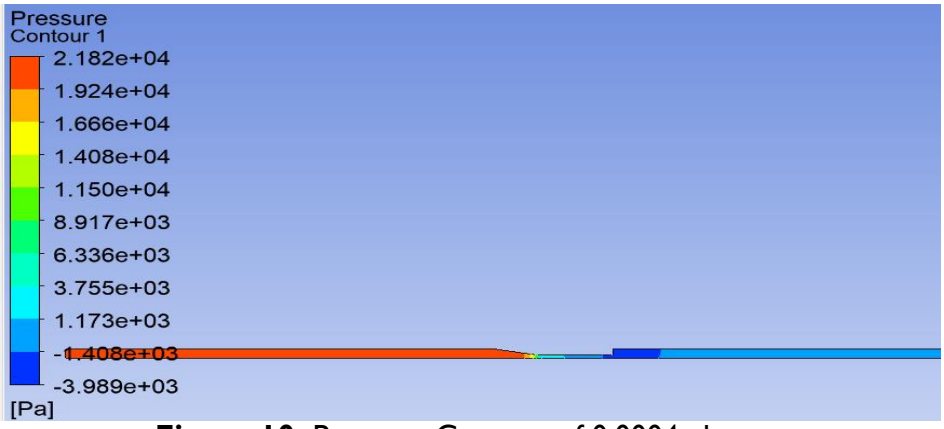

Figure 10: Pressure Contour of 0.0004 element

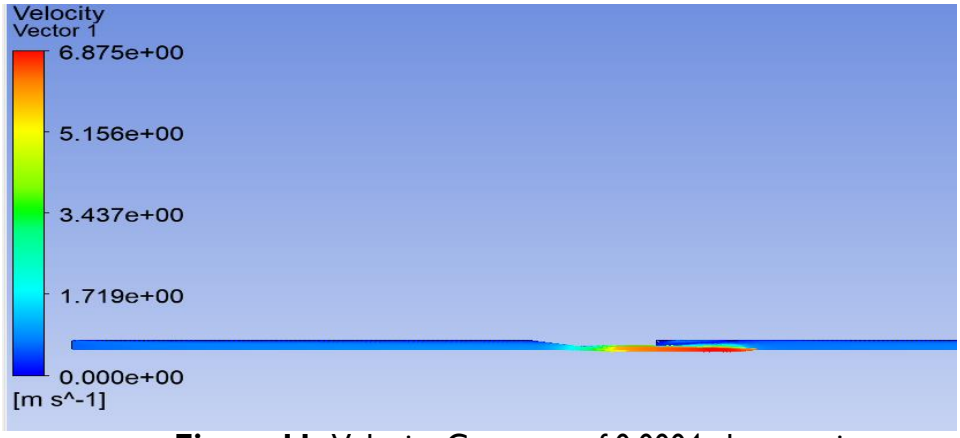

Figure 11: Velocity Contours of 0.0004 element size

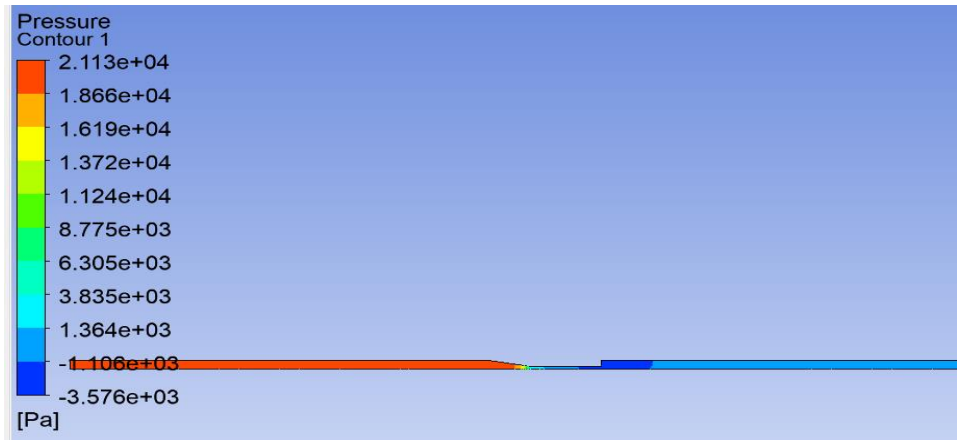

Figure 12: Pressure contour of 0.0002 element size

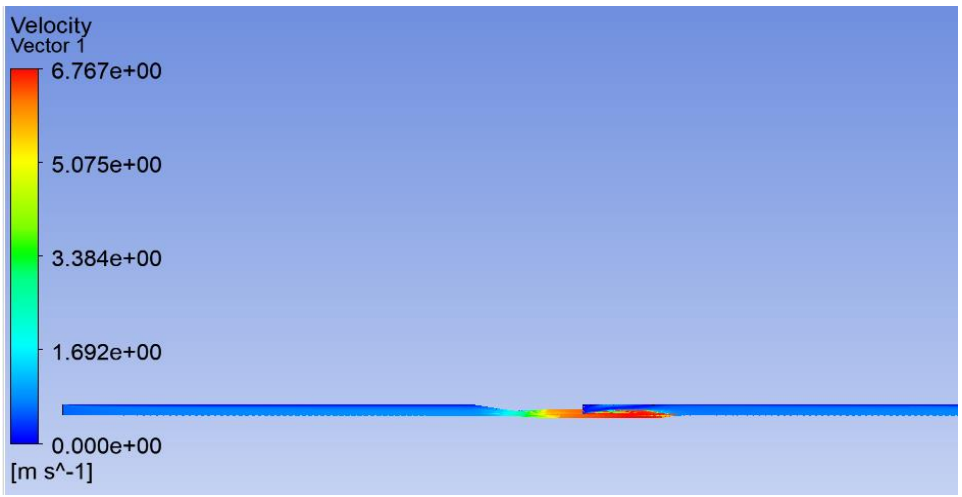

Figure 13: Velocity contours of 0.0002 element size

Figure 14 shows the mesh independence plot for the simulation, velocity against Y+. The axial velocity shows 0.016 meters after the sudden expansion. The velocity magnitude at 0.004 and 0.0002 are the same which shows the convergence of the solution.

Corresponding author's e-mail address: zubbymike@gmail.com

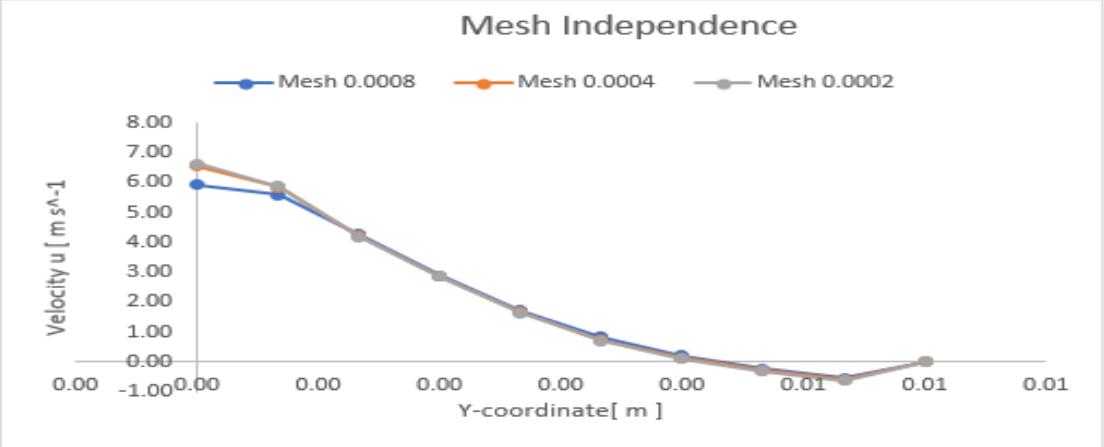

Figure 14: Mesh independence determination

Tables 5, 6 and 7 were respectively, generated from simulation showing the results of flow rate and throat and inlet Reynolds numbers. Showing the Reynolds Numbers and inlet velocities, and mesh data.

Table 5: Different flow rate throat and inlet Reynolds numbers

Flow Rate (m^3/s)	Throat Reynolds Number	Inlet Reynolds Number
5.21 x 106	500	167
2.08 x 105	2000	667
6.77 x 105	6500	2167

Table 6: Reynolds number and inlet velocities

Re	Inlet Velocity (m/s)
6500	0.5985
2000	0.1842
500	0.04613

Table 7: No of elements, nodes, element sizes and pressure drops

No of elements	Nodes	Element Size	Pressure Drop(pa)
16401	17181	0.0008	23132.2
39862	41274	0.0004	21747.4
118394	120986	0.0002	21006.8

4. Results

The results of axial velocity at the throat with Reynolds numbers 500 and 6500 after sudden expansion were discussed.

Comparative study of axial velocity models at throat Reynolds number $Re_{th.}$ = 500, after sudden expansion at line cut for various Y = 0.088m 0.024m and 0.08m with experimental data is of Stewart et al. (2012) presented in Figure 15 as

Corresponding author's e-mail address: zubbymike@gmail.com

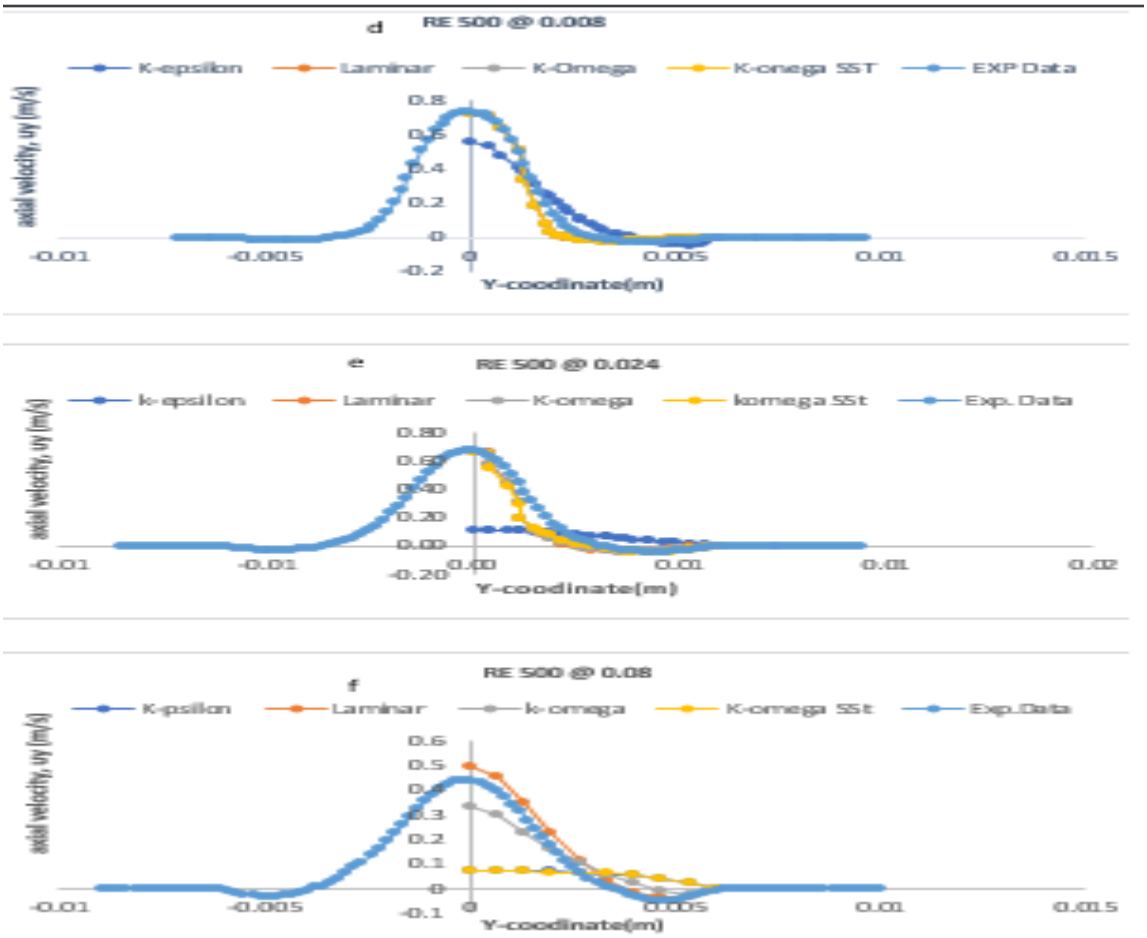

Figure 15: Axial velocity at Re_{th} = 500, after sudden expansion at line cut for various Y = 0.088m, 0.024m and 0.08m

Figures 15 d, e and f show the plots after sudden expansion for simulations of axial velocities Re_{th} = 500, Y= 0.008, 0.024, and 0.08. The simulation showed poor match with k-epsilon and K-omega SST, but laminar and K-omega matched with the experimental data at 16d and 16e. But at 16f, all showed deviation from the experimental data. This mismatch is due to participant choice of laminar model for lower Re_{th} for jets delivering after sudden expansion to be at laminar region from upstream to downstream before sudden expansion. Thus, K-omega SST and K-epsilon are possibly to be applied in area with higher Reynolds number. The line amongst the jet and recirculated zone signifies unaffected instability, but noticeable interruption at Re_{th} = 500 in our experiments was observed. Undoubtedly, at this low Re_{th}, simple turbulence models ought not to be used.

The Models comparative study of axial velocity at Re_{th}. = 6500, after sudden expansion at line cut for various Y = 0.008m, 0.024m, and 0.08m. Figure 16 shows the analysis of the throat Reynolds number 6500 axial velocity after sudden expansion.

Corresponding author's e-mail address: zubbymike@gmail.com

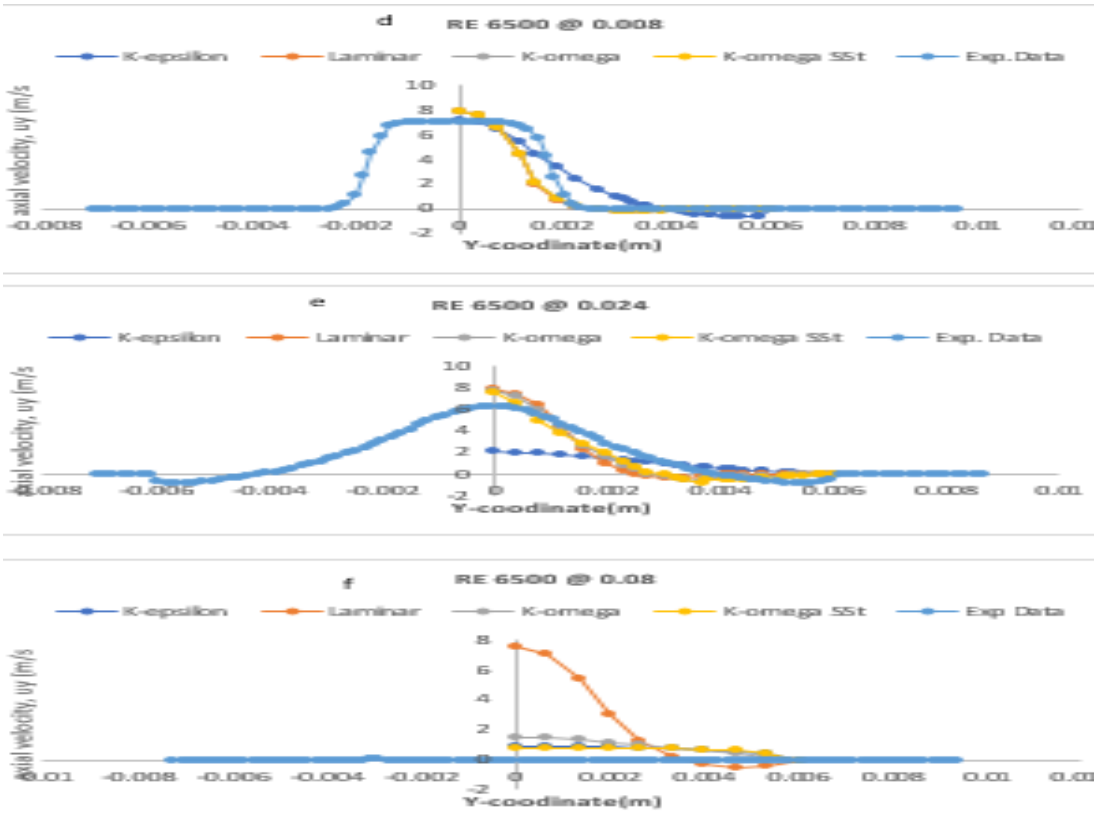

Figure 16: Axial velocity at $Re_{th.}$ = 6500, after sudden expansion at line cut for various Y = 0.008m, 0.024m, and 0.08m

From the result in Figure 16 d, e, and f, it can be seen that the experimental data at the point of downstream of the sudden expansion has 95% confident interval with k-epsilon followed by k-omega SST. This proves the fact that from upstream before sudden expansion the fluid flow regime is confirmed. Therefore, at higher Reynolds number, k-omega and Laminar departed downwards beyond downstream than experimental and disappeared. This reveals that Laminar and k-omega models are better for lower Reynolds number of Re_{th} = 500, while K-omega SST is meant for near transition of Re_{th} = 2000, and K-epsilon is best for a higher Reynolds turbulent region of Re_{th} = 6500. Thus, the study shows that RANS is particularly good for estimating transitional and turbulent flow but failed to estimate the wall pressure and axial velocity of laminar fluid flow. Furthermore, the estimation of the flow regime after the sudden expansion had a poor agreement with the experimental results. To establish CFD as a regulatory tool for medical devices its predictive capabilities for laminar flow regimes and divergent sections within a medical device need to be enhanced. Lastly, mesh refinements need to be considered as a potential solution for capturing flow patterns more accurately. Table 8 shows the percentage error associated with the wall pressure at the inlet for the three flow regimes. This showed that at the Laminar regime the wall pressure is more and decreases with an increase in the Reynolds number.

Table 8: Percentage of error for Wall Pressure at Inlet (-0.09m)

Flow conditions	Maximum Difference at -0.09m
Laminar Flow (Re =500)	19.0%
Transitional Flow (Re=2000)	17.2%
Turbulent Flow (Re=6500)	8.10%

Corresponding author's e-mail address: zubbymike@gmail.com

5. Conclusion

A 2D axisymmetric axial nozzle model geometry was created in solid works and imported to ANSYS work bench 2020R1 for simulation. Four simulation models were employed based on throat Reynolds numbers Re_{th} =500, 2000, and 6500. Mesh independence was determined using K-omega SST for 0.0008, 0.0004, and 0.0002 element sizes. However, 0.0004 element size was chosen for subsequent simulation for axial velocity at centerline, wall pressure and axial velocity at different determinations.

The result at line X=0 for Re_{th} = 500, 2000, and 6500 showed maximum difference of 77.4% for the velocity at centerline at 0.08m and 19% for the wall pressure at -0.09m sudden expansion at the region of Laminar regime of Re = 500. Besides, 65.6% and 17.2% were obtained at transition of Re = 2000, with good agreement between the CFD simulation and the experimental measurements. Meanwhile, at turbulent regime of Re = 6500, all the simulation models were in good agreement at 49.6% velocity centerline and 8.10% pressure drop, except in laminar region. Downstream of the simulation of Re_{th} = 6500, other models disappeared which demonstrated K-epsilon best for higher Reynolds number. Along wall pressure, negligible axial pressure gradient at centerline with drop in normalization point of experimental data from 0 to -120/m^2 counterbalanced at Re_{th} = 500 was observed.

This evaluation confirms the possibility of CFD simulation in analsying nozzle benchmarks of 2d axisymmetric model for blood pumps.

References

Bernsdorf, J., Harrisson, SE., Smith, SM., Lawford, PV. and Hose, DR. 2008. Applying the Lattice Boltzman Technique to Biofluids: A Novel Approach to Simulate Blood Coagulation. Computation Mathematics Application, *55(7):* 1408 - 1414. doi:https://DOI.org/10.1016/j.camwa.2007.08.007

Burgreen, GW., Antaki, ZJ. and Wu, ZJ. 2001. Holmes: Computational Fluid Dynamics as a Development Tool for Rotary Blood Pump. Artificial Organs, *25*(5): 336 - 340. DOI: 10.1046/j.1525-1594.2001.025005336.x.

Fraser,KH., Taskin, ME., Zhang, T., Griffith, BP. and Wu, ZJ. 2012. A quantitative Comparison of Mechanical Blood Damage Parameters in Rotary Ventricular Assist Device: Shear Stress, Exposure time and Hemolysis Index. Journal of Biomedical Engineering, *134*(8): 354 -367. DOI: 10.1115/1.4007092

Hariharan, P., Giarra, M. and Reddy, V. 2011. Multilaboratory Particle Image Velocimetry Analysis of the FDA Benchmark Nozzle to Support Validation of Computational Fluid Dynamics Simulations. Journal of Biomedical Engineering, *133*(4): 1334 - 1345. DOI: 10.1115/1.4003440

Herbertson,TH., Olia, SE. and Daly, A. 2015. Multilaboratory Study of Flow-Induced Hemolysis Using the FDA Benchmark Nozzle Model. Artifical Organ Proceedings, *39*,(2): 237 - 248. DOI: 10.1111/aor.12368

Huang, IC. 2018. CFD Validations with FDA Benchmarks of Medical Devices Flows. 15th International LS-DYNA Users Conference, 10-12 June, Dearborn, MI., USA., *4*(2): 75 - 95.

ISO 14708 - 5.: 2010. Implant for Surgery - Active Implantable Medical Devices Part 5. Arlington, VA, USA.

Corresponding author's e-mail address: zubbymike@gmail.com

ISO 5840 - 2.: 2015. Cardivascular Implant - Cardiac Valve Protheses part 2. VA, USA.

ISO 5840 - 3.: 2013. Cardivascular Implant - Cardiac Vlave Protheses part 3. VA, USA.

Jain , KL. 2020. Transition to Turbulence in an Oscillatory Flow Through Stenosis. Biomechanics and Modeling in Mechanobiology Proceedings, 8(2): 113 - 131.

Jain, K., Geir, R., Per-Kristian, E. and Kent-Andre, M. 2017. Direct Numerical Simulation of Transitional Hydrodynamics of the cerebrospinal Fluid in Chiari Malformation: The Role of Cranio-Vertebral Junction. International Journal of Numerical Methods and Biomedical Engineering, 7(3): 331 - 342. https://DOI.org/10.002/cnm.2853

Marsden, AL., Yuri, B., Long, CC. and Marek, B. 2014. Recent Advances in Computational Methodology for Simulation of Mechanical Circulatory Assist Devices. Wiley Interdiscipline Revise System Biomedics, 6(2): 169 -188. https://DOI.org/10.1002/wsbm.1260

Onah, TO., Nnaji, IA. and Nwankwo, AM. 2022. Evaluation of axial velocity and wall pressure models for nozzle bench mark using. GSC Advanced Engineering and Technology, 4(01): 012 - 024. doi:: https://DOI.org/10.30574/gscaet.2022.4.1.0041

Raben, JS., Hariharan, P., Ronald, R., Richard, M. and Pavlos, PV. 2016. Time-Resolved Particle Image Velocimetry Measurement with Wall Shear Stress and Uncertainty Quantification for the FDA Nozzle Model. Cardivascular Engineering Technology, 7(1): 7 - 22. DOI:10.1007/s/3239-015-0251-9

Stewart, SFC., Prasanna, H., Eric, GP., Burgreen, GW., Varun, R., Steven, WD., Matthew, G., Keefe, BM., Steven, D., Michael, RB., Matthew, RM. and Richard, AM. 2013. Results of FDA'S First Interlaboratory Computational Study of a Nozzle with a Sudden Contraction and Conical Diffuser. Cardivascular Engineering Technology proceedings, 4(4): 374 - 391.

Stewart, SC., Eric, G., Greg, W., Burgreen, P., Hariharan, P. and Matthew. T. 2012. Assesment of CFD Performance in Simulation of an Idealized Medical Device. Results of FDA'S First Computational Inter-laboratory Study, 7(3): 894 -906.

Sun, C. and Munn, LL. 2008. Lattice -Boltzmann Simulation of Blood Flow in Digitized Vessel Networks. Computation of Mathematics Application, 5(2): 1594 - 1600.

White, AT. and Chong, CK. 2011. Rotational Invariance in the Three Dimensional Lattice Boltzmann Method is Dependent on the Choice of Lattice. International Journal of Computational Physics, 3(1): 6367 -6378.

Zhang, J., Paul, CJ. and Aleksander, SP. 2008. Red Blood Cell Aggregation and Dissociation in Shear Flows Simulated by Lattice Boltzmann Method. International Journal of Biomedicals, 4(1): 47 -55. DOI:10.1016/j.jbiomech.2007.07.020

Corresponding author's e-mail address: zubbymike@gmail.com